Structural Investigations of Segmented Block Copolymers. I. The Morphology of Poly(ether Esteramide)s Based on Poly(tetramethylene Oxide) "Soft" Segments

G. PEREGO, M. CESARI, and G. DELLA FORTUNA, *Assoreni, Physical Chemistry Department, 20097 San Donato Milanese, Milano, Italy*

Synopsis

The morphology of poly(ether esteramide)s (PEEA) of the general formula $[(6NT6)_k\text{-}PTMO]_z$ has been investigated by wide and small angle X-ray scattering and electron microscopy techniques. The copolymers are based on poly(esteramide) "hard" segments (containing an average number k of 6NT6 consecutive units) alternating poly(tetramethylene oxide) (PTMO) "soft" segments of constant length (MW ~ 900). The fraction of crystallized 6NT6 increases by increasing the PTMO content (i.e., by lowering k), approaching unity for $k \to 1$. The morphology is of lamellar type, with both thickness and width of the crystalline domains (6NT6) decreasing with the increase of PTMO content; in the interlamellar amorphous regions both "soft" and "hard" segments tend to segregate in separate domains. For $k \simeq 1$, crystalline domains, formed essentially by isolated 6NT6 units, alternate with amorphous PTMO interlayers. The mechanism of evolution of the morphological structure as a function of the copolymer composition is discussed.

INTRODUCTION

Thermoplastic elastomers are copolymers generally containing two types of blocks, one of which, characterized by low glass transition temperature, is commonly referred to as the "soft" segment, since it imparts elastomeric properties to the polymer. The second component, conventionally referred to as the "hard" segment, is a rigid, generally crystallizable or glassy block, capable of forming physical crosslinks which provide for dimensional stability while preventing cold flow. The molecular weight of "hard" and "soft" blocks can be very high as in styrene–butadiene–styrene triblock copolymers, or relatively low as in segmented block copolymers (like polyurethanes) which contain "hard" and "soft" segments alternating with each other many times in the chain.

New poly(ether esteramide)s (herein referred to as PEEA), belonging to the class of segmented block copolymers, have been synthesized in our laboratories[1] by melt polycondensation of *N,N'*-bis(*p*-carbomethoxybenzoyl)hexamethylenediamine with 1,6-hexanediol and poly(tetramethylene ether) glycol (PTMEG). The wide range of the valuable physical and technological properties disclosed by these copolymers induced us to carry out an extensive investigation of their structural and morphological features. On the other hand, it was felt to be of relevant interest to make a parallel investigation on other typical elastoplastic segmented copolymers like the poly(ether ester)s obtained by polycondensation of dimethylterephthalate with 1,4-butanediol and PTMEG.

Journal of Applied Polymer Science, Vol. 29, 1141–1155 (1984)
 CCC 0021-8995/84/041141-15$04.00

In the present study we have attempted a comprehensive elucidation of the morphology of both series of copolymers, by joint application of wide- and small-angle X-ray scattering techniques and electron microscopy, enlarging our investigation to the whole compositional ranges of the copolymers. Moreover, a new notation of the molecular topology has been introduced, following a "structural" criterion instead of the conventional "chemical" one.

A partial report of this research concerning PEEA has been previously published.[2,3] It is the purpose of this paper to report the conclusive results of the investigation on the morphology of PEEA. In a second paper[4] on the morphology of poly(ether ester)s, we will draw a general comparison of the structural behaviour of both series.

DEFINITION OF THE MACROMOLECULAR STRUCTURE

According to the conventional definition,[5] PEEA are represented by the formula

$$(A_mB_n)_z \tag{1}$$

where A and B units are

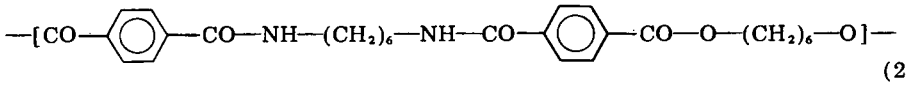

(2)

and

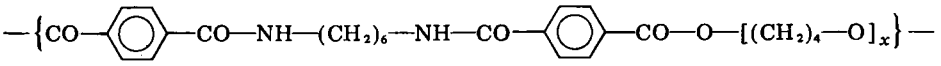

(3)

respectively. z is the polymerization degree of the copolymers, while m and n indicate the average sequence lengths of the consecutive A and B units, respectively; x is the average polymerization degree of the PTMEG used in the synthesis. A_m and B_n constitute the so-called "hard" and "soft" segments respectively. From a structural point of view this description is somehow inaccurate as A units are also contained in B units.

In order to set up the new description, let us rewrite A and B units by using proper subunits:

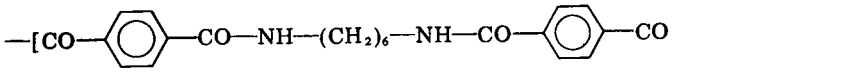

—O(CH₂)₃—(CH₂)₃O]— (4)

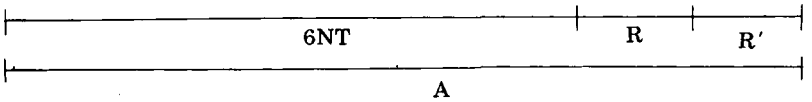

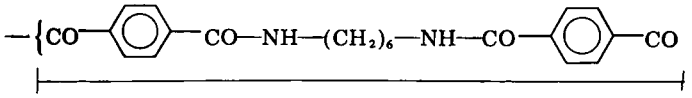

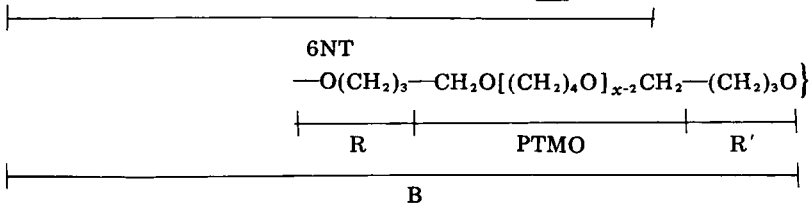

(5)

According to (4) and (5), the macromolecular chain of PEEA may be regarded as formed by sequences of R–6NT–R′ units (the distinction between R and R′ is merely formal), conventionally referred to as 6NT6,[6] separated by the PTMO unit specified in (5). In this view an A_mB_n sequence becomes $(6NT6)_{m+1}(PTMO)(6NT6\text{–}PTMO)_{n-1}$. Consequently, the whole chain may be described as

$$[(6NT6)_k\text{–}PTMO]_z \tag{6}$$

where k is the average number of consecutive 6NT6 units. From a chemical point of view, 6NT6 units are equivalent to the corresponding A units (conventional definition), but their amount increases and the block-length distribution varies when adopting the new description. However, one can verify that the average sequence length k has the same value of m (see Ref. 7).

The new description allows the separation of the true "soft" polytetramethylene oxide (PTMO) segment from the true "hard" polyesteramide 6NT6 segments. Formula (6) represents the new *structural* notation. As an example, let us rewrite a conventionally defined A_2B_2 chain segment of PEEA. Using (4) and (5), we get

$$\text{6NT—R—R}'\text{—6NT—R—R}'\text{—6NT—R—PTMO—R}'\text{—6NT—R—PTMO—R}' \tag{7}$$

It follows that, by formally transposing the right terminal R′ group at the left of (7), the structural notation becomes

$$(6NT6)_3PTMO(6NT6)PTMO \tag{8}$$

The transposition is legitimate when considering an ideal infinite chain. In the actual case of a finite chain, a terminal R (or R′) group is practically neglected in our notation, the diol or PTMEG constituting the most probable chain termination. Obviously one terminal group (diol or PTMEG) is neglected also in the conventional notation. It is evident from (7) and (8) that consecutive B units give rise to a configuration where 6NT6 units alternate perfectly with PTMO units. Therefore, the extreme compositional limits will be $(6NT6)_z$ (i.e., 6NT6 homopolymer) and the alternate configuration $(6NT6\text{–}PTMO)_z$. For sake of clarity, the symbol H will be used hereinafter to indicate the "hard" 6NT6 unit, the symbol S the "soft" PTMO unit; (6) can therefore be replaced by the general notation

$$(H_k\text{–}S)_z \tag{9}$$

EXPERIMENTAL

Materials

Samples of PEEA have been synthesized in our laboratory following a procedure previously described[1]; poly(tetramethylene ether) glycol (PTMEG) with a number average molecular weight 1000 has been used. Starting from the weight fractions of A, w_A, and B, w_B, units (conventional description) we get the weight fraction w_H and $w_S = 1 - w_H$ (new description) by the transformation formula

$$w_H = w_A + (w_B \cdot M_A/M_B) \tag{10}$$

where M_A and M_B are the molecular weights of A and B units (494.6 and 1376.4, respectively). By considering the general formula $(H_k\text{–}S)_z$, w_H can range from 0.36 (k = 1) to 1.0 (6NT6 homopolymer). The corresponding maximum content of PTMO, w_S^{max}, is therefore 0.64. The samples investigated, with w_S in the range 0–0.63, are identified by the "PEEA" label followed by the wt % of PTMO units; 6NT6 homopolymer is labelled as PEEA-0. The composition of the copolymers was determined by ^{1}H-NMR spectroscopy[8] using trifluoroacetic acid as solvent and TMS as internal standard. Two resonance regions were investigated, one (7–8 ppm from TMS) corresponding to both the aromatic and amidic hydrogens, the other (3–4 ppm) to the methylenic hydrogens in α-position with respect to —CO—NH— (3.2 ppm), —CO—O— (4.0 ppm), and —O— (3.2 ppm) groups. The mole fraction of B units is given by the formula:

$$\frac{(I_2 - 8/10\, I_1)/4}{I_1/10\,(x-1)}$$

where I_1 and I_2 are the integrated areas of the 7–8 and 3–4 ppm regions respectively and x is the polymerization degree of PTMEG. ^{13}C-NMR was employed for samples with very low content of "hard" units. In this case the evaluation of the composition was based on the resonances of the two nonequivalent quaternary aromatic carbon atoms belonging to A (135.6 and 137.6 ppm) and B units (135.9 and 137.4 ppm), respectively. The results of NMR analysis were found to be in good agreement with those expected from the composition of the reaction mixture. A list of the samples used is given in Table I.

Specimens of PEEA of dimensions 3 × 1 × 0.15 cm were obtained by compression molding at temperatures approximately 30°C above their melting points, the cooling having been performed under pressure with a rate of ca. 20°C/min. Density was measured using a conventional density gradient.

Techniques

Wide-angle (WAXS) and small-angle (SAXS) X-ray scattering measurements were performed using nickel-filtered Cu$K_{\bar{\alpha}}$ radiation. WAXS patterns were recorded by a standard Philips diffractometer equipped with a pulse height analyzer. SAXS measurements were carried out by a Kratky camera in the preset count mode, accumulating a minimum number of 10^4 counts. A step-scanning procedure was applied in the 2θ angular range 0.07–7°; the contribution of the region between 0° and 0.07° was brought into account by means of a Gaussian extrapolation. The magnitude of the primary beam was determined using a calibrated Lupolen sample provided by Professor O. Kratky. Analysis of SAXS patterns has been performed by using a computer program, written in FORTRAN language by one of us (M. C), running on IBM-VM system.

Transmission electron microscopy (TEM) observations were performed on thin sections of compression molded samples, stained by immersion for 30 min in a 0.2% aqueous solution of phosphotungstic acid (PTA). PTA is not absorbed appreciably in samples with $w_S < 0.2$ also for longer staining times, since little or no structure was evident in these samples, in spite of the presence of a definite peak in SAXS patterns. Because the stain is preferentially absorbed in the amorphous phase, crystalline domains are visible as light regions in TEM micrographs.

TABLE I
Sample Description and Experimental Data

Sample	ρ[a] (g·cm^{-3})	w_A[b]	w_H[c]	$w_{H(k)}$[d] $k=1$	2	3	>3	w_c[e] WAXS	Density	Extrap	L (Å)		$10^3\eta^2$[h]	σ^2(A^2)[i]
PEEA-0	1.250	1.0	1.0					0.44		0.44	134[f]	117[g]	1.06	13.3
PEEA-8	1.227	0.87	0.92	<0.01	<0.01	<0.01	0.91	0.43	0.46	0.43	145	124	1.58	6.4
PEEA-15	1.206	0.76	0.85	0.01	0.01	0.02	0.81	0.37	0.45	0.42	156	123	2.41	6.6
PEEA-26	1.183	0.59	0.74	0.03	0.05	0.06	0.60	0.37	0.51	0.41	170	123	3.30	5.0
PEEA-35	1.160	0.45	0.65	0.06	0.08	0.09	0.42	0.33	0.50	0.40	185	131	4.19	5.1
PEEA-42	1.141	0.35	0.58	0.09	0.11	0.10	0.28	0.32	0.47	0.39	j	j	4.53	4.6
PEEA-47	1.126	0.26	0.53	0.13	0.13	0.10	0.17	0.30	0.45	0.38	j	j	4.84	5.2
PEEA-52	1.114	0.19	0.48	0.17	0.14	0.08	0.09	0.27	0.43	0.38	j	j	4.96	5.9
PEEA-56	1.102	0.13	0.44	0.22	0.13	0.06	0.03	0.27	0.40	0.37	j	j	5.10	6.6
PEEA-59	1.094	0.08	0.41	0.26	0.11	0.03	0.01	0.28	0.39	0.37	135	98	5.40	8.8
PEEA-62	1.089	0.04	0.38	0.31	0.06	0.01	<0.01	0.23	0.38	0.36	125	93	5.35	8.7
PEEA-63	1.082	0.02	0.37	0.34	0.03	<0.01	<0.01	0.25	0.36	0.36	100	83	5.30	9.3

[a] Mass density, exptl values.
[b] Weight fraction of A units, conventional description; see text.
[c] Weight fraction of 6NT6 units, actual description; see text.
[d] Weight fractions of 6NT6 sequences containing k 6NT6 units, calculated according to Ref. 7 for infinite chain length.
[e] Crystalline weight fraction.
[f] Long spacing from desmeared SAXS curves.
[g] Long spacing from desmeared and Lorentz corrected SAXS curves.
[h] Electron density variance in (mole electrons)^2·cm^{-6}, from SAXS.
[i] Variance of the interface thickness following Ruland.[10]
[j] Not measurable because of very broad SAXS peak.

Procedures

Crystallinity. The crystalline weight fraction w_c has been evaluated by WAXS patterns following the conventional procedure[9] based on graphical separation to intensities $I_c(s)$ and $I_a(s)$, due to the crystalline and amorphous fractions of the material, respectively. The 3–34° 2θ angular region was taken into account; in this region the profile of the amorphous halo, i.e., $I_a(s)$, depends upon the relative amounts of amorphous PTMO and 6NT6. Therefore, after a rough estimation of w_c, a profile of a suitable amorphous halo was determined from a weighted overlapping of the halos typical of the pure components (PTMO, 6NT6). The calculated profile was fitted to X-ray pattern, taking advantage of some points of the pattern where the contribution of the crystalline fraction is negligible. Generally, the application of this method has to be considered satisfactory. However, for PEEA with $w_S > 0.5$, the reliability of the method is rather low, because of the large diffuseness of the reflections, which leads to a quite probable underestimation of the crystalline content.

By assuming additivity of specific volumes, w_c was also estimated from the equation

$$1/\rho = w_S/\rho_{aS} + w_c/\rho_{cH} + (1 - w_c - w_S)/\rho_{aH} \tag{11}$$

where ρ is the overall mass density of the samples, w_S a compositional value, and the density ρ_{cH} was drawn from the literature (see Table II); the density of amorphous PTMO, ρ_{aS} and the density ρ_{aH} of amorphous 6NT6 were determined by us from the corresponding homopolymers, making use of the following procedures.

In a first procedure ρ_{aH} was derived from the equation

$$1/\rho = w_c/\rho_{cH} + (1 - w_c)/\rho_{aH} \tag{12}$$

by using the value of w_c obtained from WAXS method.

In a second procedure, ρ_{aH} was calculated by means of eq. (15), using the experimental value of the electron density variance $\overline{\eta^2}$ and appropriate values of the volume fractions of crystalline and amorphous phases, derived from WAXS crystallinity as in the first procedure.

ρ_{aS} was determined by the second procedure only. The values found for ρ_{aH} and ρ_{aS} are reported in Table II.

TABLE II
Values of the Mass Densities Used in the Calculation of $\overline{\eta^2}$

ρ_{cH} = 1.316[a]	
ρ_{aH} = 1.198	(average between 1.202[b] and 1.194[c])
ρ_{aS} = 0.981	(average among 0.98[d], 0.981[e], and 0.983[f])
ρ^*_{aH} = 1.198 + 0.110w_S[g]	

[a] From structural X-ray analysis.[6]

[b] From exptl density of PEEA-0, eq. (12); see Procedures.

[c] From exptl value of $\overline{\eta^2}$ of PEEA-0, eq. (15); see Procedures.

[d] Ref. 11.

[e,f] From exptl values of $\overline{\eta^2}$ of PTMEG 1000 and 2000 MW, respectively, eq. (15); see Procedures.

[g] From the regression in Figure 3(a).

Electron Density Variance. The mean square of the electron density fluctuations, or electron density variance, $\overline{\eta^2}$, was obtained by SAXS measurements, by using the formula

$$\overline{\eta^2} = \frac{2\pi \tilde{Q}_m}{ad\lambda^3 N^2 e_0 P_0} \quad [(\text{mole-electrons})^2 \cdot \text{cm}^{-6}] \tag{13}$$

where a (cm) is the sample-receptor plane distance, d (cm) the thickness of the sample, e_0 the Thomson coefficient (7.9×10^{-26}), N the Avogadro's number, λ the wavelength used (1.5418 Å), and P_0 the integrated intensity of the primary beam. The so-called "invariant," $\tilde{Q}_m$, was obtained by the integral

$$Q_m = \int_0^\infty mI_c(m)\, dm \tag{14}$$

where m (cm) is the linear angular parameter in the receptor plane and $\tilde{I}_c$ is the experimental intensity after substraction of instrumental background and liquid scattering and after correction for the finite width of the electron density transition. The latter correction was performed by making use of the $m^3\tilde{I}(m)$-m^2 plot, following Ruland's procedure.[10]

For a multiphase system $\overline{\eta^2}$ is related to the volume fractions φ_i of the phases having a mean electron density p_i by the equation

$$\overline{\eta^2} = \sum_{i \neq j} \sum \varphi_i \varphi_j (p_i - p_j)^2 \tag{15}$$

Starting from a structural model constituted by a given number of different phases, eq. (15) allows the calculation of $\overline{\eta^2}$, provided the values φ_i and p_i are known. The comparison of the calculated value of $\overline{\eta^2}$ with the experimental one, derived as above described, can test the validity of the model assumed. The calculation of $\overline{\eta^2}$ has been performed for all of the samples of PEEA investigated by assuming two-phase and three-phase models (see Results and Discussion). The φ_i values have been derived from the chemical composition of the samples and from the crystalline fraction w_c (extrapolated values, see the next paragraph); the values of the density (from which the values of p_i can be easily derived) are those given in Table II.

When considering a mixed amorphous phase (two-phase model), additivity of specific volumes was assumed so that the density of the amorphous phase, ρ_a, was calculated as

$$1/\rho_a = (w'_S/\rho_{aS}) + (w_H - w_c)'/\rho_{aH} \tag{16}$$

the weight fractions w'_S and $(w_H - w_c)'$ being normalized to unity.

RESULTS AND DISCUSSION

Crystallinity

WAXS patterns, some of which are represented in Figure 1, show a unique crystal phase typical of 6NT6 homopolymer[6]; no crystallization of PTMO is detected. A remarkable anisotropic effect is observed in WAXS patterns: by increasing w_S, i.e., by shortening the average length of 6NT6 segments, the $0kl$ reflections maintain a sharp form, but others, in particular the $1\bar{1}0$ and 002 re-

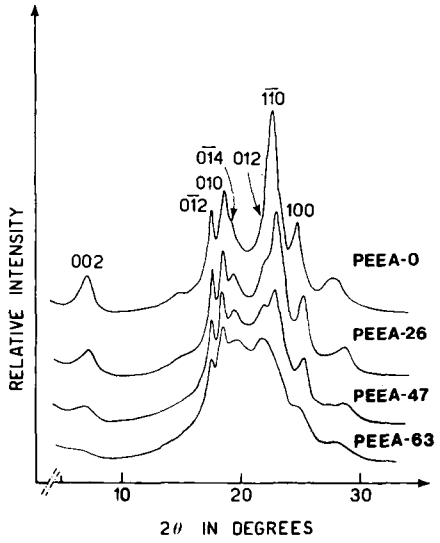

Fig. 1. Smooth traces of WAXS patterns of 6NT6 homopolymer (PEEA-0) and typical poly(ether esteramide)s. The *hkl* indices are indicated for the main reflections.

flections, tend to broaden, especially for $w_S > 0.5$. The phenomenon may be well understood by considering that the crystal structure of 6NT6 is built up of layers, constituted in turn by chain molecules interconnected by CO···HN hydrogen bonds running parallel to the $(1\bar{1}0)$ crystallographic plane, and approximately perpendicular to the (010) plane.[6] It is therefore reasonable to expect a preferential growing of the crystals along the layers rather than along the perpendicular direction. Moreover, the broadening of 002 reflection is accounted for by the reduction of the crystal size in the direction parallel to the chain axis, as a consequence of the crystallization of 6NT6 isolated units, the content of which increases rapidly for $w_S > 0.5$ (see Table I). Because of this effect too, the application of the conventional method of the graphical separation of the intensities (see Procedures) can provide only a particular estimation of crystallinity, i.e., a "crystallinity" which includes mostly well-ordered and large paracrystals. Owing to the complexity of WAXS patterns, we did not attempt a more sophisticated analysis of the patterns, but some adjustment of the w_c values, obtained by this method, was performed on the basis of other experimental data.

From Table I and Figure 2(a) it is evident that the values of w_c obtained by density method, eq. (11), are systematically higher than those drawn from WAXS method.

Considering now the crystallinity from density for PEEA-63, which has a composition very close to that of the alternating $(H–S)_z$ configuration, one can remark that the value $w_c = 0.36$ agrees well with the complete crystallization of 6NT6 present in the copolymer ($w_H = 1–0.63 = 0.37$). Because this value is confirmed also by SAXS measurements, as we will see hereinafter, the w_c value of 0.25 from WAXS must be considered too low, whatever is the model taken into account for crystallinity.

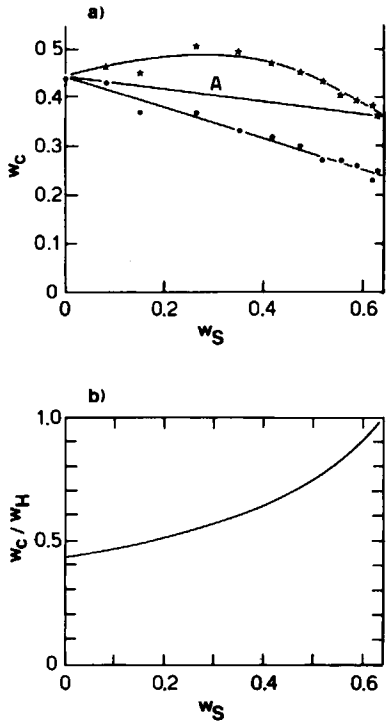

Fig. 2. (a) Crystallinity in poly(ether esteramide)s: from density (★); from WAXS (●); and extrapolated (straight line A), see text. (b) Fraction of crystallized 6NT6, w_c/w_H, deduced from straight line A, vs. the weight fraction of PTMO.

On the other hand, the bow shown by the w_c curve from the density [Fig. 2(a)] may be explained by postulating that the increased flexibility of the macromolecular chain induced by the soft PTMO segments allows the formation of small, partially ordered domains of 6NT6, which display a density higher than that of the effective amorphous 6NT6 homopolymer (ρ_{aH}). In the Hosemann's theory[12] these domains correspond to very small and low-order microparacrystals: it is questionable whether such microparacrystals have to be ascribed to the "crystalline" or the "amorphous" fraction. Our choice has been to add them to the "amorphous" fraction; consequently, the "crystalline," fraction has been assumed to decrease linearly from 0.44 (6NT6 homopolymer) to 0.36, following the straight line A in Figure 2(a).

Starting from these extrapolated values of w_c and those of the overall density, one may calculate the density of the "amorphous" 6NT6, ρ^*_{aH}, for each copolymer composition by using eq. (11). ρ^*_{aH} increases linearly with w_S [see Fig. 3(a)], which means that 6NT6 segments arrange themselves in the pseudo-amorphous domains or low-order microparacrystals in a tighter and tighter way without reaching complete crystalline order with the exception of the compositions close to w_S^{max}.

Using the same w_c values, the relative fraction of crystalline 6NT6, w_c/w_H, is given as a function of w_S [see Fig. 2(b)], showing explicitly the complete crystallization of 6NT6 near to w_S^{max}.

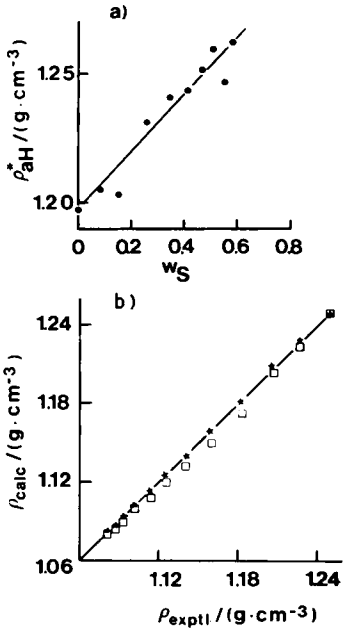

Fig. 3. (a) Mass density of amorphous 6NT6, ρ^*_{aH} from eq. (11) (●) vs. the weight fraction of PTMO. (b) Calculated overall density by eq. (11) from ρ_{aH} (□) and ρ^*_{aH} (★) vs. experimental overall density.

Nature of "Amorphous" Fraction

The model so far discussed, disregarding the topological organization of the phases, should be constituted by a "crystalline" phase, formed by highly ordered and generally large crystals of 6NT6, and a so-called "amorphous" phase containing PTMO and domains of residual 6NT6 with different degrees of order. This three-phase model may be compared to a two-phase model, constituted by crystalline 6NT6 and a true amorphous phase arising from a homogeneous mixing of the remaining fraction of 6NT6 and PTMO.

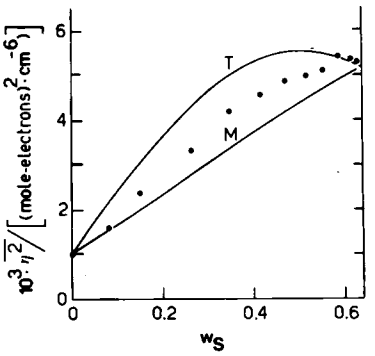

Fig. 4. Experimental (●) and calculated (two-phase, curve M, and three-phase, curve T, structures) values of the electron density variance vs. the weight fraction of PTMO.

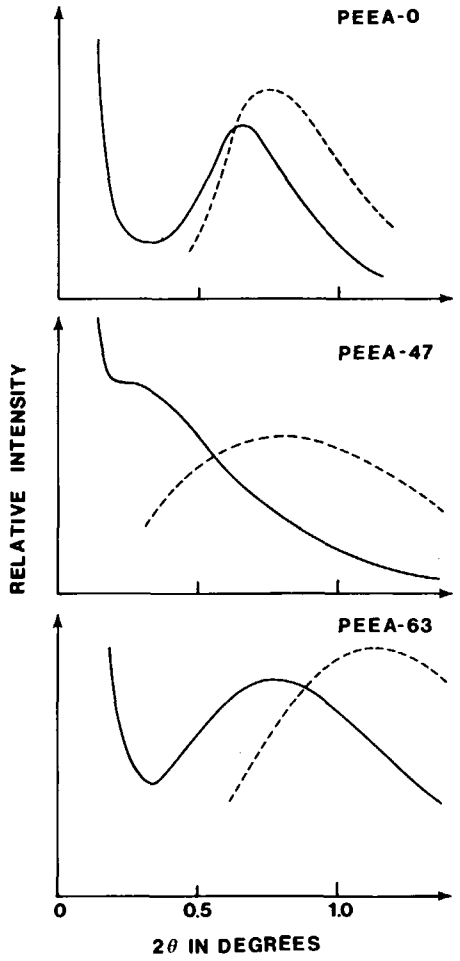

Fig. 5. SAXS patterns of 6NT6 homopolymer (PEEA-0) and typical poly(ether esteramide)s; desmeared (—) and desmeared and Lorentz-corrected (- - -) SAXS curves.

In order to get a further insight on the constitution of the so-called "amorphous" fraction, we have compared the values of the electron density variance, $\overline{\eta^2}$, measured by SAXS method, with the calculated ones for the two-phase and three-phase models (see Procedures); ρ_{aH} and ρ^*_{aH} values were used in the calculation of $\overline{\eta^2}$ for the two models, respectively. In any case, the alternative choice of ρ_{aH} or ρ^*_{aH} leads to negligible differences in the calculated values of $\overline{\eta^2}$ in both cases. However, it is worth remarking that the values used in eq. (15) for calculating $\overline{\eta^2}$ fit the experimental values of the overall density of the corresponding sample; only when ρ_{aH} (instead of ρ^*_{aH}) is employed, slight but systematic discrepancies between experimental and calculated values are observed (see Fig. 3(b)]. For sake of clarity, the calculated values of $\overline{\eta^2}$ have been reported in form of curves (see Fig. 4), instead of discrete points, after a smoothing procedure has been applied (curves M and T for two-phase and three-phase models, respectively). Experimental $\overline{\eta^2}$ values continuously increase as a function of w_S and the final points fit well the model in which almost all the isolated 6NT6 units

(a)

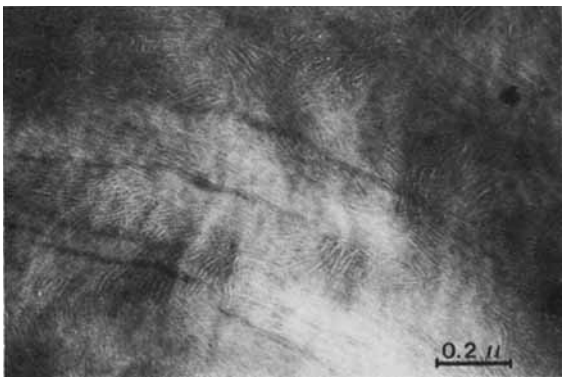

(b)

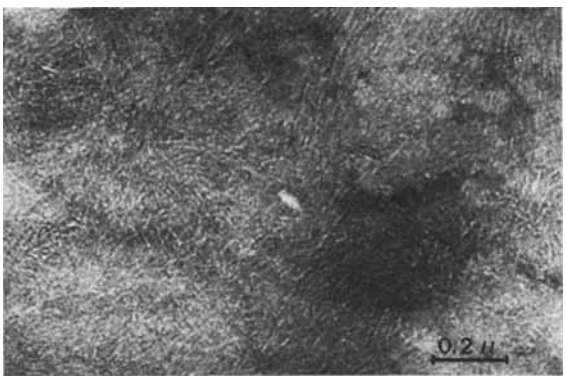

(c)

Fig. 6. Transmission electron micrographs of thin sections of compression molded PEEA-26 (a), PEEA-42 (b), and PEEA-59 (c) samples.

crystallize. Nevertheless, by excluding this extreme points where the two-phase and three-phase models coincide, the experimental values are located approximately in the middle between the T and M curves. This behavior indicates a tendency towards a three-phase model, particularly for $w_S > 0.2$, although some 6NT6 units homogeneously mixed with PTMO units are also present; however, this fraction becomes negligible at high PTMO content. It is worth mentioning

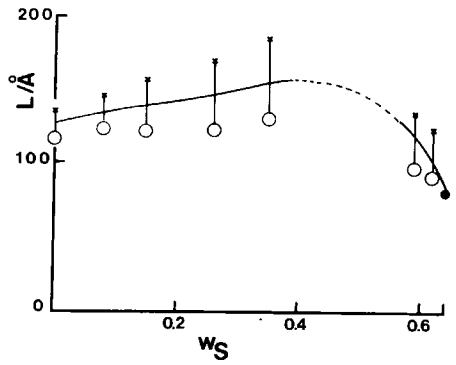

Fig. 7. Long spacing L from desmeared (x) and desmeared and Lorentz corrected (O) SAXS curves, vs. the weight fraction of PTMO. Calculated value for the ideal alternate $(H–S)_z$ structure (●); see Table III.

that phase separation in the amorphous part of PEEA is also evident by dynamic mechanical measurements.[2]

We presume that effects of partial ordering involving the PTMO segments are quite unlikely.

Morphological Organization of the Phases

Experimental SAXS patterns, some of which are reproduced in Figure 5, show one peak, more or less broadened, along almost all the compositional range. Starting from a well-defined peak (PEEA-0), a progressive broadening in addition to a slight displacement towards smaller angles is observed by increasing w_S up to ca. 0.4. In the range 0.4–0.6 a nearly continuous scattering is observed, but again a rather well-defined peak, displaced towards higher angles, reappears for compositions approaching the extreme w_S value 0.64.

TEM micrographs show a lamellar-type morphology (see Fig. 6) for all the composition range. However, a true lamellar organization, with lateral dimensions of 2000–3000 Å or more, is observed for the lowest w_S values only, while evolution to a pseudolamellar structure, set up by smectic-like arrangements of microparacrystals 200–300 Å wide, occurs for the highest w_S values.

The mean period L, the so-called "long spacing," of the monodimensional structure in which "crystalline" lamellae alternate "amorphous" interlayers, may be in principle derived by SAXS peak, by simple application of the Bragg's law. Nevertheless, the derivation of the reliable and accurate values for L is not straightforward, being the application of an appropriate Lorentz factor to SAXS curve rather uncertain and still questioned in literature.[13] Moreover, the form of the correction gives rise to very different values of L just when the peak is broad and its maximum position is difficult to define. For this reason, we have taken into account the L values deduced from both simply desmeared and desmeared and Lorentz-corrected SAXS curves, assuming the Lorentz factor proportional to the square of the angular parameter; no L values are reported for the case of too large peaks (see Table I and Fig. 7). In the range of w_S, 0–0.4, L slightly increases; when w_S approaches w_S^{max}, L clearly decreases towards the value of 81 Å, expected for a structure where crystalline domains of isolated 6NT6 units

TABLE III
Structural Data for the Ideal Alternate $(H–S)_z$ Copolymer

Lamellar thickness corresponding to one 6NT6 unit, d_{001} of the crystal lattice,[a] l_c = 24 Å
Cross section of 6NT6 (crystal)[a]: 26.03 Å^2
Mass density of amorphous PTMO,[b] ρ_{aS} = 0.981 g·cm^{-3}
Volume occupied by an amorphous PTMO segment, 881.8 MW,[c] $V_S = 881.8 \times 1.66/0.981 = 1492.1$ Å^3
Average thickness of an amorphous PTMO layer (1 segment per cross section of 6NT6), $l_S = 1492.1/26.03 = 57.3$ Å
Long spacing expected for the $(H–S)_z$ configuration, $L = l_c + l_S = 24 + 57.3 = 81.3$ Å

[a] Ref. 6.
[b] See Table II.
[c] Resulting from the difference between MW of the B unit and MW of 6NT6; see text.

alternate amorphous PTMO interlayers. The value of 81 Å was calculated following the scheme reported in Table III.

By assuming the lamellar structure to be volume-filling, the thickness of crystalline lamellae, l_c, is derived from L by $l_c = L \cdot \varphi_c$, where φ_c is the volume fraction of lamellae, easily obtained by w_c. In the w_S range 0–0.4, l_c corresponds to the value expected for 2–3 6NT6 monomeric units, 48–72 Å, depending on the choice of L; l_c decreases for $w_S > 0.6$, tending to the value of 24 Å calculated for the alternating $(H–S)_z$ structure (see Table III).

The trend displayed by SAXS patterns in terms of peak broadening may be understood by considering the structural evolution occurring with the increase of w_S. The lamellae progressively become smaller and smaller microparacrystals while in the "amorphous" interlayers the pseudo-amorphous domains of 6NT6 evolve continuously towards low-order microparacrystals. The formation of these pseudo-amorphous domains, connected to the neighbor microparacrystals by PTMO segments of constant length, provoke the disalignment of the microparacrystals so as to progressively destroy the regularity of the lamellar-type structure, with the consequent disappearance of the SAXS peak (w_S = 0.4–0.6). The evolution proceedes until the composition of the $(H–S)_z$ configuration is approached, resulting in the formation of uniform low-order microparacrystals; in this composition range ($w_S > 0.6$) the structure is practically built up of these microparacrystals regularly alternating PTMO interlayers; consequently, a sharp SAXS peak reappears. This behavior should be hardly understood without admitting the occurrence of a three-phase structure.

Further comments will be given in a subsequent paper[4] where the morphology of PEEA is compared to that of the poly(ether ester)s based on the same PTMO "soft" segment.

The authors are indebted to Professor E. Cernia and to Professor R. Hosemann for helpful criticisms and discussions. Thanks are due to Dr. C. Corno for NMR analysis.

References

1. E. Sorta and G. della Fortuna, *Polymer*, **21**, 728 (1980).
2. G. della Fortuna, A. Melis, G. Perego, R. Vitali, and L. Zotteri, Proceedings of the International Rubber Conference, Venice, 1979, p. 229.

3. A. Biggi, G. della Fortuna, G. Perego, and L. Zotteri, *Kautschuk Gummi, Kunststoffe*, **34,** 349 (1981).

4. G. Perego, M. Cesari, and R. Vitali, *J. Appl. Polym. Sci.*, **29,** 1157–1169 (1984).

5. W. H. Buck, R. J. Cella, Jr., E. K. Gladding, and J. R. Wolfe, Jr., *J. Polym. Sci., Polym. Symp.*, **48,** 47 (1974).

6. M. Cesari, G. Perego, and A. Melis, *Eur. Polym. J.*, **12,** 585 (1976).

7. E. Sorta and A. Melis, *Polymer*, **19,** 1153 (1978).

8. C. Corno, unpublished results.

9. L. E. Alexander, *X-ray Diffraction in Polymer Science*, Wiley-Interscience, New York, 1969.

10. W. Ruland, *J. Appl. Crystallogr.*, **4,** 70 (1971).

11. D. W. Van Krevelen, *Properties of Polymers, Correlations with Chemical Structure*, Elsevier, New York, 1972.

12. R. Hosemann, *Makromol. Chem. Suppl.*, **1,** 559 (1975).

13. B. Crist and N. Morosoff, *J. Polym. Sci., Polym. Phys. Ed.*, **11,** 1023 (1973).

Received March 15, 1983
Accepted September 17, 1983